TLM-Based Modal-Extraction Approach for the Investigation of Discontinuities in the Rectangular Waveguide and the NRD

Bratin Ghosh, Neil R. S. Simons, Lotfollah Shafai, *Fellow, IEEE*, Apisak Ittipiboon, *Member, IEEE*, and Aldo Petosa, *Member, IEEE*

***Abstract*—This paper describes the development of a rigorous transmission-line matrix-based modal-extraction approach to analyze discontinuities in guided-wave structures in general, with particular attention to the nonradiative dielectric waveguide (NRD). The motivation for this paper arose from the need to ascertain the admittance of a slot in the ground plane of an NRD without relying on experimental data. These data enabled one to design an NRD-based slot array following the methodology of Malherbe, Malherbe *et al.*, and Ghosh *et al.*. Previous work in this area relied on placing observation points sufficiently remote from the discontinuity in order to ensure the decay of scattered evanescent modes to appreciably low levels. The method discussed here obviates this requirement and allows the evaluation of generalized scattering-matrix coefficients arbitrarily close to the discontinuity, thus significantly reducing the computational overhead. Results pertaining to discontinuities in the NRD and the rectangular waveguide have been presented and shown to give good agreement with those in the literature and with measurements. The perfectly matched layer has been used as an absorbing boundary condition in our simulations. Finally, the results have been verified using the power-conservation and Poynting's theorems.**

***Index Terms*—Discontinuities, modal extraction, NRD, PML, TLM.**

I. Introduction

THE nonradiative dielectric waveguide (NRD) has been recognized as an effective transmission medium for millimeter waves because of its intrinsic low-loss nature and its unique ability to suppress radiation from bends and discontinuities due to the separation between its ground planes being less than half a free-space wavelength. The above properties of the NRD have made it possible to develop NRD-based components with extremely low-loss, reduced interference, easy integrability with active devices, and ease of manufacture with increased mechanical tolerances, especially in the millimeter-wave range. Time-domain methods like the transmission-line matrix (TLM) are particularly suited for the analysis of NRD-based components and discontinuities because of the inhomogeneity of the structure of the NRD guide and the hybrid and complex nature of its modes. In this paper, we describe the development and application of a rigorous and efficient analytical tool based on the TLM algorithm similar to the one used in conjunction with the finite-difference time-domain (FDTD) method in [4] for the analysis of discontinuities in the NRD guide. Previous results obtained using the TLM algorithm in the analysis of discontinuities in guided-wave structures like the rectangular waveguide [5] required placement of observation surfaces sufficiently remote from the discontinuity to ensure the attenuation of evanescent waves scattered from the discontinuity to an appreciable extent. Also, results in [5] have been presented for the case where only the dominant mode is above cutoff. The technique described in this paper, i.e., the TLM-based modal-extraction approach, enables the extraction of scattering-matrix parameters arbitrarily close to the discontinuity, thus reducing the size of the computational domain and simulation time. It also allows the evaluation of the generalized scattering-matrix coefficients of all scattered modes. Furthermore, the technique can be readily extended to the investigation of discontinuities in any kind of guided-wave structure. Results obtained using this tool for several types of discontinuities in the NRD including the slot in the NRD ground plane have been presented and verified with those in the literature and with measurements. Good agreement has been noticed for both. The latter results demonstrate that an NRD-based slot array can be designed taking into account mutual coupling using the methodology in [1]–[3] without recourse to empirical data. Moreover, it was found that lateral power flow through the edges of the NRD ground planes have to be considered to validate our results using power-conservation and Poynting's theorems. Two types of discontinuities in the rectangular waveguide have also been treated using our approach. It was also found that the perfectly matched layer (PML) had to be used as an absorbing boundary condition to obtain adequate absorption levels for the cases under study. The introduction of the PML obviates the need for precomputation and large memory overheads involved in storing a time-domain Green's function, [6], [7] though the PML parameters have to be properly chosen to avoid instabilities.

Manuscript received June 17, 2001.

B. Ghosh and L. Shafai are with the Department of Electrical and Computer Engineering, University of Manitoba, Winnipeg, MB, Canada R3T 5V6.

N. R. S. Simons is with Market Risk Trading and Insurance, Royal Bank of Canada, Toronto, ON, Canada M5J 2J5.

A. Ittipiboon is with the Communications Research Center, Ottawa, ON, Canada K2H 8S2 and also with the Department of Electrical and Computer Engineering, University of Manitoba, Winnipeg, MB, Canada R3T 5V6.

A. Petosa is with the Communications Research Center, Ottawa, ON, Canada K2H 8S2 and also with the Department of Electronics, Carleton University, Ottawa, ON, Canada K1S 5B6.

Digital Object Identifier 10.1109/TMTT.2002.803429.

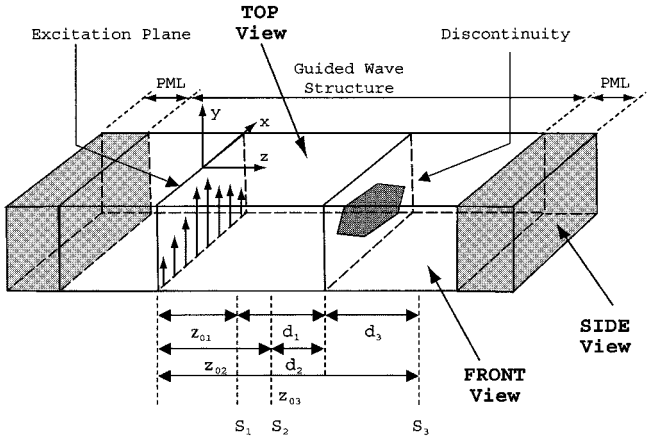

Fig. 1. General configuration of the simulation space for the TLM analysis of a discontinuity in a guided-wave structure.

II. Theory

In this section, the formulation of the TLM-based modal-extraction approach is discussed. The computational domain for a discontinuity in a general guided-wave structure is shown in Fig. 1. Electromagnetic waves, originating from the excitation plane, propagate down the guided-wave structure and get scattered from the discontinuity. The computational domain was terminated by PMLs on either sides to reduce the reflection from the boundaries down to extremely low levels. Observation surfaces S_1, S_2, and S_3 used to extract the modes incident and scattered from the discontinuity can be located arbitrarily close to the discontinuity.

The general expression of the transverse electric field in the frequency domain $E_{t\text{-inc}}(\omega)$ obtained from the TLM simulation engine at any location in the guided-wave structure to the left-hand side (incident) of the discontinuity is as shown in (1) at the bottom of this page. In the above, A_{00} and B_{00} refer to the amplitudes of the incident and reflected modes, while B_{mn} refers to the amplitude of the reflected mode of order mn. It may be noted that the incident mode might or might not be the dominant mode for the guided-wave structure under consideration. Also, β_{00} denotes the propagation constant of the incident mode, while β_{mn} denotes the propagation constant of the mode of order mn. The function $\psi_{abcde}(x, y)$ describes the transverse variation of fields at any cross section in the guided-wave structure. The subscripts used in this notation, which are valid for the rest of this paper, are explained as follows.

- Subscript "a" can assume the values of "0" to "m" where "0" refers to the eigenvalue of the guided-wave structure in the "x" direction of the incident mode and "m" to that of the mth higher order mode in the "x" direction.
- Subscript "b" can assume the values of "0" to "n" where "0" refers to the eigenvalue of the guided-wave structure in the "y" direction of the incident mode and "n" to that of the nth higher order mode in the "y" direction.
- Subscript "c" can be either "x" or "y" and refers to the "x" or "y" component of the field, respectively.
- Subscript "d" can be either "e" or "h" and refers to the electric or magnetic field components, respectively.
- Subscript "e" can be either "i" or "r" and refers to a wave traveling in the same direction as the incident or reflected wave, respectively.

When (1) is evaluated at a surface S_1 at a location $z = z_{01}$ on the left-hand side of the discontinuity, (2) is obtained, as shown at the bottom of this page. The unknowns in (2), *viz.* A_{00}, B_{00}, and B_{mn}'s, can be determined by applying the Lorentz reciprocity theorem as described below. To determine A_{00} and B_{00}, a test magnetic field on surface S_1 is defined as follows:

$$H_{T00i}(\omega)|_{(z=z_{01})} = \begin{bmatrix} \widehat{u_x}\psi_{00xhi}(x, y)e^{-j\beta_{00}z_{01}} \\ + \\ \widehat{u_y}\psi_{00yhi}(x, y)e^{-j\beta_{00}z_{01}} \end{bmatrix}. \quad (3)$$

$$E_{t\text{-inc}}(\omega) = A_{00}\left[\widehat{u_x}\psi_{00xei}(x, y)e^{-j\beta_{00}z} + \widehat{u_y}\psi_{00yei}(x, y)e^{-j\beta_{00}z}\right] + B_{00}\begin{bmatrix} \widehat{u_x}\psi_{00xer}(x, y)e^{j\beta_{00}(z-(z_{01}+d_1))-j\beta_{00}(z_{01}+d_1)} \\ + \\ \widehat{u_y}\psi_{00yer}(x, y)e^{j\beta_{00}(z-(z_{01}+d_1))-j\beta_{00}(z_{01}+d_1)} \end{bmatrix} + \sum_{m=1}^{\infty}\sum_{n=1}^{\infty} B_{mn}\begin{bmatrix} \widehat{u_x}\psi_{mnxer}(x, y)e^{j\beta_{mn}(z-(z_{01}+d_1))-j\beta_{00}(z_{01}+d_1)} \\ + \\ \widehat{u_y}\psi_{mnyer}(x, y)e^{j\beta_{mn}(z-(z_{01}+d_1))-j\beta_{00}(z_{01}+d_1)} \end{bmatrix} \quad (1)$$

$$E_{t\text{-inc}}(\omega)|_{(z=z_{01})} = A_{00}\begin{bmatrix} \widehat{u_x}\psi_{00xei}(x, y)e^{-j\beta_{00}z_{01}} \\ + \\ \widehat{u_y}\psi_{00yei}(x, y)e^{-j\beta_{00}z_{01}} \end{bmatrix} + B_{00}\begin{bmatrix} \widehat{u_x}\psi_{00xer}(x, y)e^{-j\beta_{00}z_{01}-2j\beta_{00}d_1} \\ + \\ \widehat{u_y}\psi_{00yer}(x, y)e^{-j\beta_{00}z_{01}-2j\beta_{00}d_1} \end{bmatrix} + \sum_{m=1}^{\infty}\sum_{n=1}^{\infty} B_{mn}\begin{bmatrix} \widehat{u_x}\psi_{mnxer}(x, y)e^{-j\beta_{mn}d_1-j\beta_{00}(z_{01}+d_1)} \\ + \\ \widehat{u_y}\psi_{nnyer}(x, y)e^{-j\beta_{mn}d_1-j\beta_{00}(z_{01}+d_1)} \end{bmatrix} \quad (2)$$

In (3), the subscripts used in the notation $H_{Tabc}(\omega)$ are valid throughout this paper and are explained as follows.

- Subscript "T" denotes "test field."
- Subscript "a" can assume the values of "0" to "m" where "0" refers to the eigenvalue of the guided-wave structure in the "x" direction of the incident mode and "m" refers to that of the mth higher order mode in the "x" direction.
- Subscript "b" can assume the values of "0" to "n" where "0" refers to the eigenvalue of the guided wave structure in the "y" direction of the incident mode and "n" to that of the nth higher order mode in the "y" direction.
- Subscript "c" can be either "i" or "r" and refers to a wave traveling in the same direction as the incident or reflected wave, respectively.

The integral

$$\iint_{S_1} \left(E_{t\text{-inc}}(\omega) \times H_{T00i}(\omega)\right) \bullet \widehat{u_z}\, dS$$

is computed using (2) and (3). It can be observed that, because of orthogonality, the only terms that remain on the right-hand side are those involving A_{00} and B_{00}, yielding an equation of the following form:

$$\iint_{S_1} \left(E_{t\text{-inc}}(\omega) \times H_{T00i}(\omega)\right) \bullet \widehat{u_z}\, dS = f_1(A_{00}, B_{00}). \quad (4)$$

Using the same technique on another surface S_2 at a location $z = z_{02}$, which might be located in close proximity to the surface S_1, another equation similar to (4), involving A_{00} and B_{00} is obtained. Solving these two equations, the two unknowns A_{00} and B_{00} can be determined. To determine B_{mn}, a test magnetic field is defined on surface S_1 as follows:

$$H_{Tmni}(\omega)|_{(z=z_{01})} = \begin{bmatrix} \widehat{u_x}\psi_{mnxhi}(x, y)e^{-j\beta_{mn}z_{01}} \\ + \\ \widehat{u_y}\psi_{mnyhi}(x, y)e^{-j\beta_{mn}z_{01}} \end{bmatrix}. \quad (5)$$

The expression

$$\iint_{S_1} \left(E_{t\text{-inc}}(\omega) \times H_{Tmni}(\omega)\right) \bullet \widehat{u_z}\, dS$$

is evaluated using (2) and (5), where, again, because of orthogonality, a function involving only B_{mn} remains on the right-hand side as follows:

$$\iint_{S_1} \left(E_{t\text{-inc}}(\omega) \times H_{Tmni}(\omega)\right) \bullet \widehat{u_z}\, dS = f_2(B_{mn}). \quad (6)$$

Equation (6) can be solved for B_{mn}.

A similar approach was used to determine the amplitudes of the scattered modes on the right-hand side (transmitted) of the discontinuity at the observation surface S_3.

Some reduction in computation can be achieved while using the above formulation to extract the scattered longitudinal section electric (LSE) modes generated by discontinuities in the NRD by using the transverse magnetic fields from the TLM code. It is advantageous to use the transverse electric field as the test field in this case, as the electric field of the LSE modes lie entirely tangential to the air–dielectric interface.

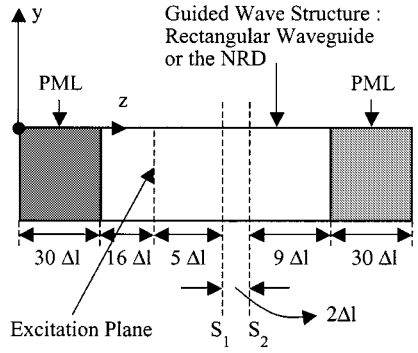

Fig. 2. Guided-wave structure (front view) with observation surfaces S_1 and S_2 terminated by PMLs on both sides.

III. Results

A. Performance of the PML in the Rectangular Waveguide and the NRD

The PML had to be used as an absorbing boundary condition in our simulations, as traditionally used boundary conditions like the matched condition for normal incidence, which has been proven effective in terminating TEM structures like the microstrip, yielded a reflection coefficient only of the order of -5 dB when used for terminating non-TEM structures like the rectangular waveguide or the NRD. The PMLs, implemented in the manner suggested in [8] and [9], were chosen to have a thickness of 30 cells, a geometric profile of conductivity of geometric ratio 3.16, and a theoretical reflection coefficient of 0.01, and used in terminating both the rectangular waveguide and the NRD in our simulations (Fig. 2). These PMLs are denoted by the notation (30-G3.16-0.01). The rectangular waveguide (cross section: 3.5574 mm $\times$ 7.1148 mm) and the NRD (distance between the ground planes $a = 15.20$ mm, width of dielectric $b = 9.60$ mm, and dielectric constant of dielectric $\varepsilon_r = 2.55$) were excited with the dominant TE_{10} mode and the LSM_{01} mode, respectively. A spatial discretization (Δl) of 0.1078 mm was used for the case of the rectangular waveguide, while $\Delta l = 0.80$ mm was used in the case of the NRD. Fig. 3 shows the results for the reflection coefficient computed using the modal-extraction approach, treating the PML on the right-hand side as a discontinuity. It can be seen that S_{11} values in excess of -50 dB can be obtained for the rectangular waveguide, as well as the NRD; thus demonstrating that the PML can be used as an effective absorbing boundary condition in case of both.

B. Discontinuities in the Rectangular Waveguide

Two types of discontinuities in the rectangular waveguide, *viz.* a capacitive iris and a half-filled metal plate, are considered here [10]. For both cases, $\Delta l = 0.1078$ mm was used in the simulations. For the 25–40-GHz frequency range under investigation, the TE_{10} dominant mode was the only propagating mode in the rectangular waveguide.

1) Capacitive Iris in a Rectangular Waveguide: Fig. 4 shows the configuration of the iris of gapwidth $d = 1.1858$ mm

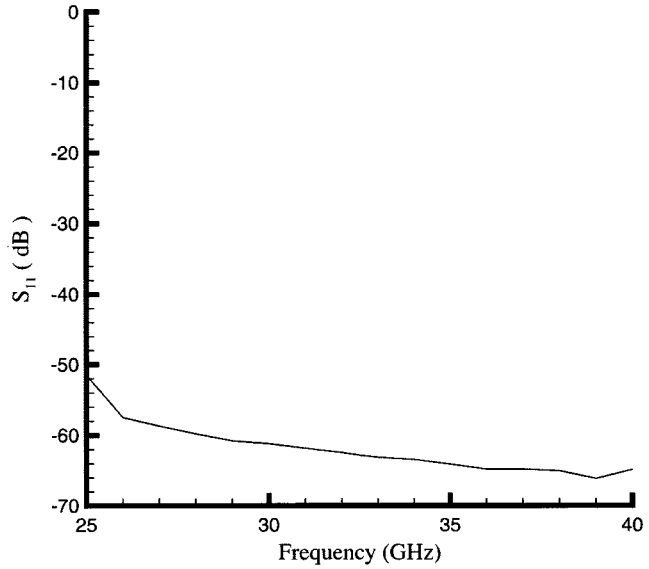

(a)

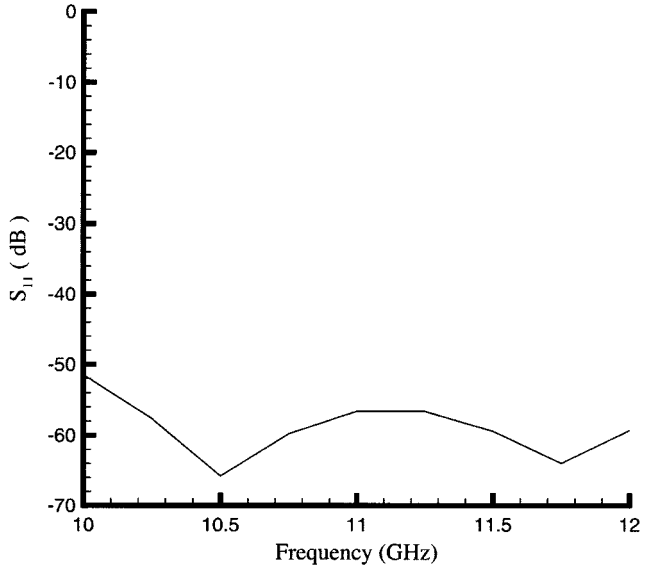

(b)

Fig. 3. S_{11} versus frequency for a rectangular waveguide and NRD terminated by PMLs on both sides. (a) Rectangular waveguide. (b) NRD.

in a 3.5574 mm $\times$ 7.1148 mm rectangular waveguide and the computational domain for determining its scattering-matrix parameters using the modal-extraction approach. In order to verify the technique, two sets of observation surfaces were used on the left-hand side of the discontinuity. The local observation surfaces, *viz*. observation surfaces 2 spaced $2\Delta l$ apart, were placed at a distance of $\lambda_g/22.47$ $(=5\Delta l)$ from the discontinuity, while remote observation surfaces, *viz*. observation surfaces 1 also spaced $2\Delta l$ apart, were placed at a distance of $\lambda_g/1.20$ $(=94\Delta l)$ from the discontinuity, λ_g being the guide wavelength of the TE_{10} mode at the center frequency of 32.50 GHz. (30-G3.16-0.01) PMLs were used in the simulations. Fig. 5 shows good agreement between the results of the magnitude and phase of the reflection coefficient at the local and remote observation surfaces. However, a difference can be noted between the TLM simulation results

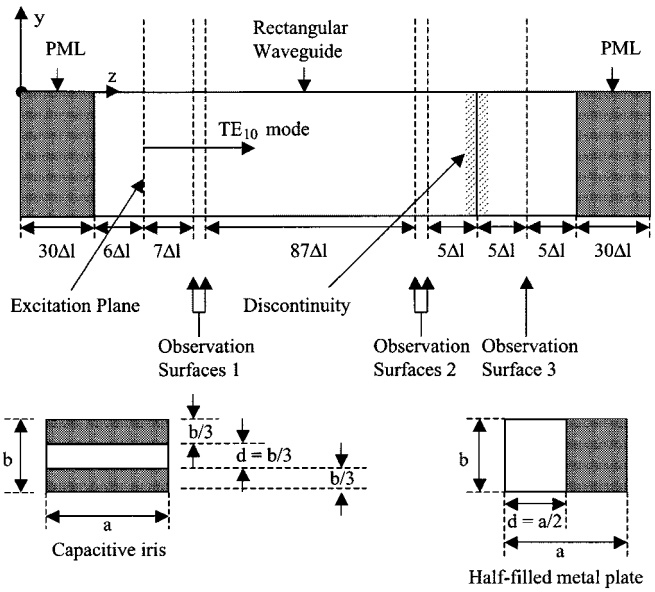

Fig. 4. Computational domain (front view) for extraction of scattering-matrix parameters in the case of a capacitive iris in a rectangular waveguide.

and the benchmark solution [11] in Fig. 5(a). This difference has been noted in [5], and can be attributed to the inability of the TLM method to model the rapid spatial variation in the field distribution in the vicinity of the singularity at the edge of the iris [12]. As regards the difference between the TLM results and the benchmark solution in the value of the phase of the reflection coefficient [see Fig. 5(b)], a finer mesh was shown to reduce the discrepancy between the two in [5].

In addition, checking was done for conservation of power for the incident and scattered waves at the local observation surfaces [see Table I(a)]. A third observation surface, *viz*. observation surface 3 located $5\Delta l$ from the discontinuity (Fig. 4), was also used to extract the amplitude of the transmitted dominant mode using the modal-extraction approach for this purpose. The following notations have been used in this and all subsequent tables in this paper:

- IPm — incident power on the left-hand side of discontinuity, computed using the modal-extraction approach;
- RPm — reflected power on the left-hand side of discontinuity, computed using the modal-extraction approach;
- TPm — transmitted power on the right-hand side of discontinuity, computed using the modal-extraction approach;
- SPm — total scattered power computed using the modal-extraction approach $= \mathrm{RPm} + \mathrm{TPm}$;
- IPmnet — net power flow on the left-hand side of discontinuity, computed using the modal-extraction approach;
- IPtnet — real part of net power flow on the left-hand side of discontinuity, computed using Poynting's theorem;
- OPtnet — real part of net power flow on the right-hand side of discontinuity, computed using Poynting's theorem;
- LPt — real part of net power flow through lateral surface on the left-hand side (when looking forward

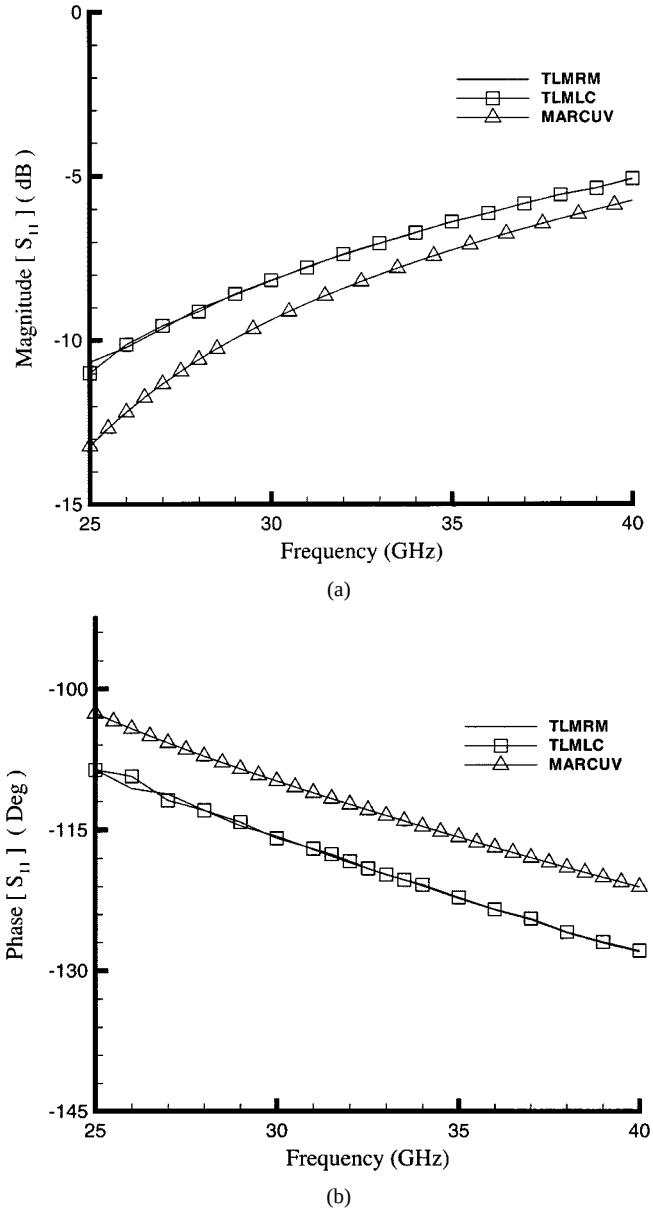

Fig. 5. S_{11} versus frequency for a capacitive iris. TLMLC: TLM simulation results at local observation surfaces. TLMRM: TLM simulation results at remote observation surfaces. MARCUV: Benchmark solution from [11]. (a) Magnitude. (b) Phase.

along the direction of propagation), computed using Poynting's theorem;

RPt real part of net power flow through lateral surface on the right-hand side (when looking forward along the direction of propagation), computed using Poynting's theorem;

Rrad real part of radiated power from the slot, computed using Poynting's theorem.

According to the theorem of conservation of power, the power in the incident wave must equal the sum of the powers of all the propagating modes in the scattered waves, which consists of the reflected and transmitted waves in this case. Table I(a) shows reasonable convergence in the results of this check.

An additional check was conducted by comparing the net power flow using Poynting's theorem [13] with those computed using the modal-extraction approach at the local observation surface on the left-hand side of the discontinuity [see Table I(b)]. The computations using Poynting's theorem were performed by using the fields as directly output by the TLM simulation engine at the observation surface. It is again seen that a reasonable agreement exists between the modal-extraction approach and Poynting's theorem.

TABLE I
VERIFICATION OF POWER CONSERVATION IN THE CASE OF A CAPACITIVE IRIS IN A RECTANGULAR WAVEGUIDE. (a) CONSERVATION FOR INCIDENT AND SCATTERED POWERS USING ONLY MODAL-EXTRACTION APPROACH. (b) COMPARISON OF NET POWER FLOW ON THE LEFT-HAND SIDE OF DISCONTINUITY COMPUTED USING MODAL-EXTRACTION APPROACH AND POYNTING'S THEOREM

Frequency (GHz)	IPm (Watts)	SPm (Watts)	X (%)
29.00	1.00487E-02	1.00474E-02	1.25490E-02
33.00	1.00168E-02	1.00231E-02	6.36795E-02
37.00	1.00322E-02	1.00400E-02	7.77851E-02

(a)

Frequency (GHz)	IPmnet (Watts)	IPtnet (Watts)	X (%)
29.00	8.66150E-03	8.64576E-03	0.182058
33.00	8.03373E-03	8.01927E-03	0.180312
37.00	7.42042E-03	7.40789E-03	0.169144

(b)

In order to compare the computing resources needed for the modal-extraction approach with those required in a standard TLM simulation, the simulation parameters for both have been shown in Table II. The simulations were run on a Sun Blade 1000 workstation with a 750-MHz UltraSPARC III CPU. The computational domain in Fig. 4 was shrunk by $89\Delta l$ along the z-axis by removing observation surfaces 1 and the region between the observation surfaces 1 and observation surfaces 2 while evaluating the TLM-based modal-extraction approach. Table II shows that a considerable improvement in CPU times can be achieved using the modal-extraction approach. For all other simulations discussed in this paper, only observation surfaces located close to the discontinuity were used for extracting modal amplitudes of the incident and scattered modes.

2) Half-Filled Metal Plate in a Rectangular Waveguide: In this section, power-conservation results with the iris in the previous section replaced with a half-filled metal plate in the rectangular waveguide has been presented. The computational domain shown in Fig. 4, which was used in the case of the iris in the rectangular waveguide, was used again in this case without the observation surfaces 1 and region between observation surfaces 1 and observation surfaces 2. Thus, on the left-hand side of the discontinuity, two observation surfaces spaced $2\Delta l$ apart were placed $\lambda_g/22.47$ $(=5\Delta l)$ from the discontinuity, λ_g being the guide wavelength at 32.50 GHz. The observation surface on the right-hand side of the discontinuity was also placed $5\Delta l$ from the discontinuity.

TABLE II
COMPARISON OF THE MESH SIZE, NUMBER OF TIME STEPS AND CPU TIMES FOR THE TLM-BASED MODAL-EXTRACTION APPROACH WITH STANDARD TLM

	TLM based Modal Extraction Approach	Standard TLM
Mesh Size in Δl	69 x 36 x 90	69 x 36 x 179
Number of time-steps	2800	3200
CPU time	41 min. 23.2 sec.	1 h. 38 min. 8.2 sec.

TABLE III
VERIFICATION OF POWER CONSERVATION IN THE CASE OF A HALF-FILLED METAL PLATE IN A RECTANGULAR WAVEGUIDE. (a) CONSERVATION FOR INCIDENT AND SCATTERED POWERS USING ONLY MODAL-EXTRACTION APPROACH. (b) COMPARISON OF NET POWER FLOW ON THE LEFT-HAND SIDE OF DISCONTINUITY COMPUTED USING MODAL-EXTRACTION APPROACH AND POYNTING'S THEOREM

Frequency (GHz)	IPm (Watts)	SPm (Watts)	X (%)
29.00	1.00309E-02	1.00128E-02	0.179805
33.00	1.00213E-02	1.00451E-02	0.237271
37.00	1.00515E-02	1.03491E-02	2.96141

(a)

Frequency (GHz)	IPmnet (Watts)	IPtnet (Watts)	X (%)
29.00	1.46883E-03	1.46353E-03	0.360834
33.00	2.48525E-03	2.50462E-03	0.779403
37.00	3.85019E-03	3.96581E-03	3.002970

(b)

Results involving conservation of power for the incident and scattered waves in the case of the half-filled metal plate discontinuity ($d = 3.5574$ mm) in a 3.5574 mm $\times$ 7.1148 mm rectangular waveguide are discussed in Table III(a). It can be seen that the convergence is not as good as results in case of the iris discontinuity in Table I(a). Table III(b) in this case, corresponding to Table I(b) in the case of the iris discontinuity and computed at the same observation surfaces as in Table III(a) also shows that the convergence of results in case of the iris discontinuity are better as regards net power flow on the left-hand side of the discontinuity.

C. Discontinuities in the NRD

In the following section, several discontinuities in the NRD, including the NRD slot, have been characterized using the modal-extraction approach [14]. The NRD ground plane width was chosen large enough so that the field amplitudes at the edges of the ground plane were down to negligible levels for the incident mode and all scattered modes. The matched condition for a normal incidence absorbing boundary condition was used at the edges of the ground planes and PMLs were used at either ends of the NRD. However, lateral power flow through the edges of the ground plane of the NRD in a direction normal to the air–dielectric interface was noticed for these cases, as shown in Fig. 6. This sideways leakage of power could possibly be due to the distance between the NRD ground planes being more than half a free-space wavelength at the frequency range under investigation. Coupling between higher order modes like the LSM_{31} with the equivalent slab mode, as discussed in [15]

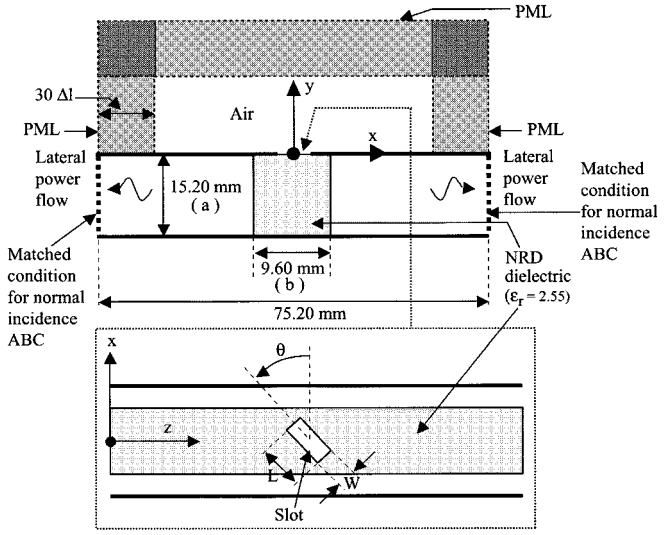

Fig. 6. Configuration of a slot in the NRD ground plane (side view on top, top view at the bottom).

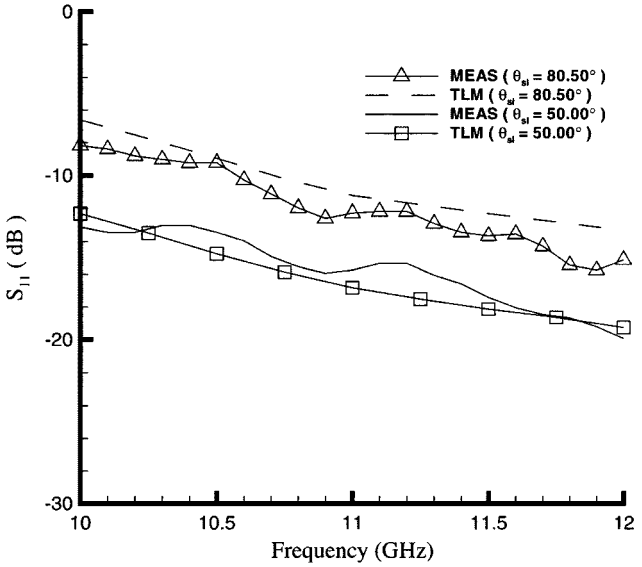

Fig. 7. S_{11} versus frequency for a slot in the NRD ground plane computed using the modal-extraction approach (TLM) and comparison with measurements (MEAS).

TABLE IV
VERIFICATION OF POWER CONSERVATION IN THE CASE OF A SLOT IN THE NRD GROUND PLANE. (a) CONSERVATION FOR INCIDENT AND SCATTERED POWERS COMPUTED AT OBSERVATION SURFACES LOCATED AT DISTANCES OF $\lambda_g/2.78$ FROM THE DISCONTINUITY. (b) CONSERVATION FOR INCIDENT AND SCATTERED POWERS COMPUTED AT OBSERVATION SURFACES LOCATED AT DISTANCES OF $2.57\lambda_g$ FROM THE DISCONTINUITY. (c) CONSERVATION FOR INCIDENT AND SCATTERED POWERS COMPUTED AT OBSERVATION SURFACES LOCATED AT DISTANCES OF $\lambda_g/2.78$ FROM THE DISCONTINUITY USING ONLY POYNTING'S THEOREM

Frequency (GHz)	IPm (Watts)	RPm (Watts)	TPm (Watts)	LPt (Watts)	RPt (Watts)	Rrad (Watts)	X (%)
10.00	1188.98	288.498	465.273	36.3738	40.8745	213.955	13.7808
11.00	1199.04	99.0479	820.837	24.3184	31.8743	97.4877	11.6877
12.00	1186.11	62.3494	951.459	14.4193	22.9614	62.4357	6.50893

(a)

Frequency (GHz)	IPm (Watts)	RPm (Watts)	TPm (Watts)	LPt (Watts)	RPt (Watts)	Rrad (Watts)	X (%)
10.00	1188.92	287.387	468.197	102.0512	105.758	210.100	1.31461
11.00	1197.53	95.7639	832.034	74.2526	79.1098	95.3076	1.79027
12.00	1185.17	56.7201	962.707	39.1968	55.9358	57.7265	1.09904

(b)

Frequency (GHz)	IPtnet (Watts)	OPtnet (Watts)	LPt (Watts)	RPt (Watts)	Rrad (Watts)	X (%)
10.00	819.769	534.884	36.3738	40.8745	213.955	0.770741
11.00	1020.93	866.964	24.3184	31.8743	97.4877	2.79807E-02
12.00	1083.86	979.341	14.4193	22.9614	62.4357	0.435758

(c)

and [16], could also probably be another cause of this power leakage.

1) Slot in the NRD Ground Plane: Fig. 6 shows the configuration of the slot in the NRD ground plane. The NRD ($a = 15.20$ mm, $b = 9.60$ mm, $\varepsilon_r = 2.55$) was excited with the LSM_{01} mode. (30-G3.16-0.01) PMLs were used to terminate the NRD on either side and (30-G2.15-0.01) PMLs were used as absorbing boundaries in the air region above the slot. $\Delta l = 0.80$ mm was used in the simulation. Fig. 7 shows the results for extraction of the reflection coefficient of the LSM_{01} mode from the slot (slot length $L = 11.20$ mm, slot width $W = 1.60$ mm) at observation surfaces spaced $2\Delta l$ apart and located $\lambda_g/2.78$ ($=14\Delta l$) from the discontinuity using the modal-extraction approach and comparison with measurements, λ_g being the guide wavelength of the LSM_{01} mode at the center frequency of 11 GHz. Two different slot inclination angles ($\theta = 80.50°$ and $\theta = 50.00°$) were considered. It can be seen that the simulation results agree with measurements reasonably well.

These results were checked for conservation of power, which implies that the incident power in the LSM_{01} mode must be equal to powers in the reflected and transmitted waves in all the propagating modes plus the real part of the radiated power through the slot. For the frequency range under consideration, the propagating modes were the LSE_{00}, LSE_{01}, and LSM_{01}.

Table IV(a) shows the conservation of power for the slot ($L = 11.20$ mm, $W1.60 =$ mm, $\theta = 89.0°$) in the NRD ($a = 15.20$ mm, $b = 9.60$ mm, $\varepsilon_r = 2.55$) ground plane in which the modal-extraction approach has been used to compute the incident and scattered powers from the slot and Poynting's theorem to compute the lateral power flow and radiated power. For this case, the modal amplitudes of the incident and scattered waves in the modal-extraction approach have been evaluated at observation surfaces located at distances of $\lambda_g/2.78$ from the slot. Large discrepancies can be noticed, especially at lower frequencies, which might be caused due to not considering the complete lateral power flow through the edges of the NRD ground planes. To verify this, the net power flow at several surfaces on the incident and transmitted sides located at varying distances from the slot were computed using the modal-extraction approach and Poynting's theorem and the results compared. Fig. 8 shows the convergence of the two approaches as the observation surfaces move further from the slot. It can be seen that the results using the two methods approach close to each other with increasing distance of the observation surfaces from the slot. Table IV(b) also shows the results for the power conservation when the observation surfaces were placed $2.57\lambda_g$ ($=100\Delta l$) from the slot. The convergence is now seen to be better than in Table IV(a), as the complete lateral power flow has been taken into consideration.

Table IV(c) shows the results when the Poynting's theorem was used to verify conservation of power for the NRD slot using observation surfaces at $\lambda_g/2.78$ from the slot, taking into ac-

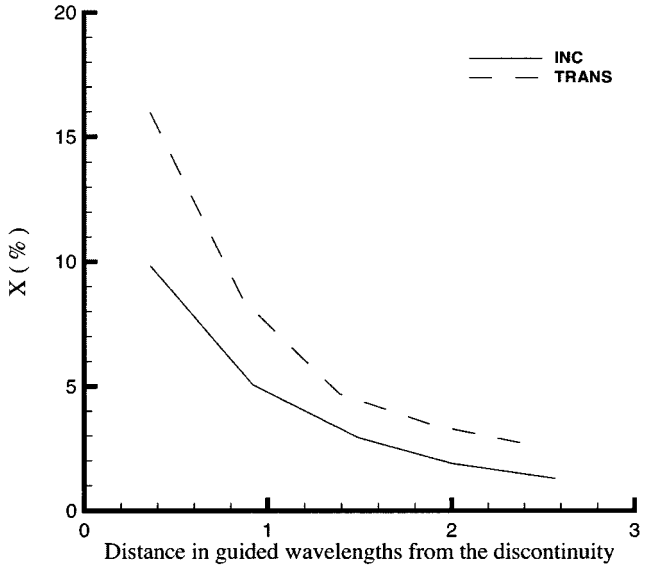

Fig. 8. Convergence between the modal-extraction approach and Poynting's theorem in the computation of net power flow in the case of an NRD slot. X: Maximum percent difference between the modal-extraction approach and Poynting's theorem over 10–12 GHz at the spatial location of the abscissa. INC: Incident side of discontinuity. TRANS: Transmitted side of discontinuity.

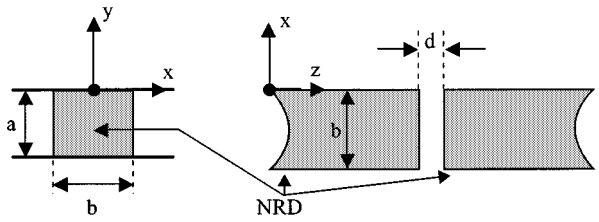

Fig. 9. Configuration of the gap discontinuity in the NRD with gapwidth d (side and top view).

TABLE V
VERIFICATION OF POWER CONSERVATION IN THE CASE OF A GAP DISCONTINUITY IN THE NRD. (a) CONSERVATION FOR INCIDENT AND SCATTERED POWERS USING ONLY POYNTING'S THEOREM, WITHOUT TAKING INTO ACCOUNT LATERAL POWER FLOW. (b) CONSERVATION FOR INCIDENT AND SCATTERED POWERS USING ONLY POYNTING'S THEOREM, TAKING INTO ACCOUNT LATERAL POWER FLOW

Frequency (GHz)	IPtnet (Watts)	OPtnet (Watts)	X (%)
10.00	1111.16	1108.44	0.25
11.00	1105.81	1089.46	1.50
12.00	1094.88	1049.84	4.29

(a)

Frequency (GHz)	IPtnet (Watts)	OPtnet (Watts)	LPt (Watts)	RPt (Watts)	X (%)
10.00	1111.16	1108.44	1.31207	1.31037	8.78945E-03
11.00	1105.81	1089.46	8.07233	8.15794	1.08415E-02
12.00	1094.88	1049.84	21.8664	21.9890	0.108320

(b)

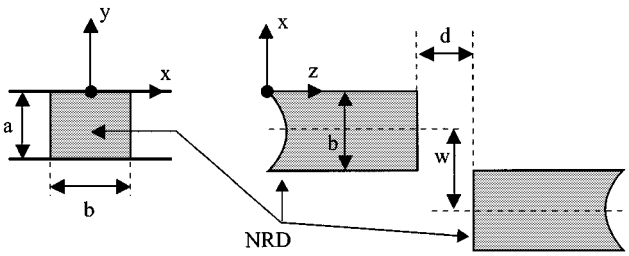

Fig. 10. Configuration of the offset gap discontinuity in the NRD with gapwidth "d" and offset "w" (side and top view). For this geometry, $w = b$.

count the lateral power flow. In this case, power conservation can be checked by verifying that the net power flow on the left-hand side of the discontinuity equals the sum of the net power flow on the right-hand side together with the lateral power flows and the radiated power. It can be seen that a good degree of convergence was achieved, as expected, as energy cannot be lost in the TLM mesh.

2) Gap Discontinuity in NRD: The next type of discontinuity in the NRD examined, called the gap discontinuity, consists of an air gap in the NRD dielectric (shown in Fig. 9). An NRD with the same geometrical and physical parameters and operating in the same frequency range as in Section III-C-1 has been used in this case with the gapwidth $d = 3.20$ mm. Thus, the only modes above cutoff are the LSE_{00}, LSE_{01}, and LSM_{01}. $\Delta l = 0.80$ mm was also used in this case. Lateral power flow also in the case of this discontinuity is apparent upon examination of Table V(a) and (b) with observation surfaces located at distances of $\lambda_g/2.99$ ($=13\Delta l$) to the left-hand side and $\lambda_g/2.59$ ($=15\Delta l$) to the right-hand side of the discontinuity, λ_g being the guide wavelength of the LSM_{01} mode at 11 GHz. Table V(a) verifies power conservation using Poynting's theorem only, but without taking into account lateral power flow. It is seen that the effect of leakage manifests in the increasing difference between the net power flows on the incident and transmitted sides of the gap discontinuity at higher frequencies, which should otherwise be equal by the power-conservation theorem, differing by as much as 4.29% at 12 GHz. However, Table V(b) shows that when the lateral power flow is added to the scattered power on the transmitted side of the gap discontinuity, the sum closely approaches the net power flow on the incident side of the discontinuity, as required by the power-conservation theorem.

3) Offset Gap Discontinuity in NRD: As a further check to the modal-extraction approach, the technique was applied to analyze an offset gap discontinuity in the NRD, as shown in Fig. 10. The results are shown in Fig. 11(a)–(d). For all these cases, the NRD ($a = 5.00$ mm, $b = 3.60$ mm, $\varepsilon_r = 2.56$) was excited with the LSM_{01} mode and the scattering-matrix parameters computed both for the reflected and transmitted LSM_{01} and the LSE_{01} modes. $\Delta l = 0.20$ mm was chosen for the simulations. In these figures, the following notation has been used.

- $|S_{11mm}|$ denotes the reflection coefficient of the LSM_{01} mode.
- $|S_{11em}|$ denotes the reflection coefficient of the LSE_{01} mode.
- $|S_{21em}|$ denotes the transmission coefficient of the LSE_{01} mode.
- $|S_{21mm}|$ denotes the transmission coefficient of the LSM_{01} mode.

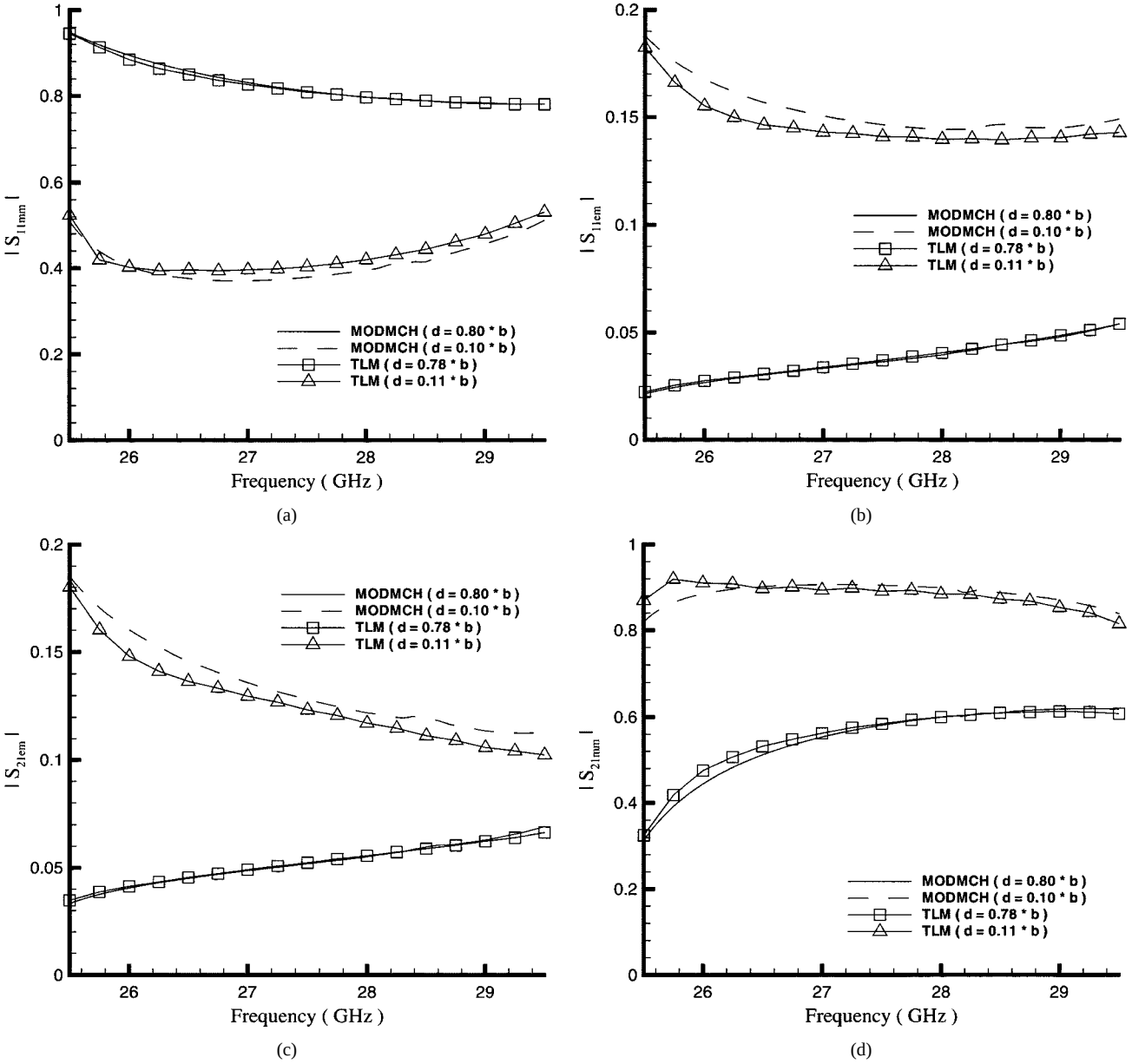

Fig. 11. Variation of the magnitude of scattering parameters with frequency for offset gap discontinuity in the NRD. (a) $|S_{11mm}|$. (b) $|S_{11em}|$. (c) $|S_{21em}|$. (d) $|S_{21mm}|$.

The offset "w" was maintained to be the same as the width of the NRD dielectric "b" in all cases. Two different values for the gapwidth "d" were chosen in the TLM simulations: $d = 0.78*b$ and $d = 0.11 * b$. The results from the TLM simulation (TLM) have been compared to those obtained using the mode-matching method (MODMCH) [17], the latter using $d = 0.80 * b$ and $d = 0.10 * b$, respectively. The gapwidth "d" in the TLM simulations had to be chosen slightly different from that used in the mode-matching method due to the discretization in the TLM lattice. For the case $d = 0.78 * b$, two observation surfaces spaced $2\Delta l$ apart were placed at a distance of $\lambda_g/3.55$ ($=27\Delta l$) to the left-hand side and another observation surface was also placed at a distance of $\lambda_g/3.55$ to the right-hand side of the discontinuity, λ_g being the guide wavelength of the LSM_{01} mode at 27.50 GHz. For the case $d = 0.11 * b$, two observation surfaces on the left-hand side spaced $2\Delta l$ apart were located at a distance of $\lambda_g/4.56$ ($=21\Delta l$) from the discontinuity and the observation surface on the right-hand side was placed at a distance of $\lambda_g/4.35$ ($=22\Delta l$) from the discontinuity. Good agreement can be seen between the results using the TLM-based modal-extraction approach and the mode-matching method.

Table VI(a) and (b) presents power-conservation results for the offset gap discontinuity ($d = 2.80$ mm, $w = 3.60$ mm), computed at the observation surfaces located at distances of $\lambda_g/3.55$ from the discontinuity. For the frequency range under consideration, the only propagating modes are the LSE_{00}, LSE_{01}, and LSM_{01}. At the highest frequency (29.5 GHz) under consideration, the free-space wavelength λ_0 is 10.17 mm. The distance between the NRD ground planes being 5.00 mm ($<\lambda_0/2$), the cutoff condition in the air region of the NRD is maintained over the 25.5–29.5-GHz frequency range. Consequently, less leakage occurs compared to the gap discontinuity

TABLE VI
VERIFICATION OF POWER CONSERVATION IN THE CASE OF AN OFFSET GAP DISCONTINUITY IN THE NRD. (a) CONSERVATION FOR INCIDENT AND SCATTERED POWERS USING ONLY POYNTING'S THEOREM (b) CONSERVATION FOR INCIDENT AND SCATTERED POWERS USING ONLY THE MODAL-EXTRACTION APPROACH

Frequency (GHz)	IPtnet (Watts)	OPtnet (Watts)	X (%)
25.50	67.5555	65.8461	2.59605
27.50	223.159	222.155	0.451936
29.50	254.603	254.532	2.78940E-02

(a)

Frequency (GHz)	IPm (Watts)	RPm (Watts)	TPm (Watts)	X (%)
25.50	639.693	572.210	68.5265	0.163128
27.50	648.352	425.075	222.969	4.75251E-02
29.50	669.862	410.136	250.501	1.39639

(b)

or NRD slot case, as is evident from Table VI(a) and (b). Table VI(a) shows that power conservation could be verified to within approximately 2.60% using Poynting's theorem without considering lateral power flow. Table VI(b) demonstrates that the maximum error in verifying power conservation using the modal-extraction approach in the near field of the discontinuity is only approximately 1.40% without taking into account the lateral power flow.

IV. CONCLUSION

Results relating to the characterization of several types of discontinuities in the rectangular waveguide and the NRD using the TLM-based modal-extraction approach have been presented in this paper. It was shown that the generalized scattering-matrix coefficients of a discontinuity in any type of guided-wave structure can be extracted in the presence of evanescent modes in the near field of a discontinuity, resulting in considerable reduction in computational effort, both in terms of simulation space and time. However, in guided-wave structures where the modes cannot be expressed as an infinite series of discrete modes, or where the modes are continuous, we might have to solve complex integral equations if the modal-extraction approach is applied to characterize discontinuities. In structures where the modes can be expressed as a infinite series of discrete modes, the modal-extraction approach is easier to apply, as has been shown in this paper. The results obtained show good agreement with those in the literature and reasonable agreement with measurements. Additionally, the power-conservation and Poynting's theorems have been used in the verification of these results. Thus, the usefulness of the TLM-based modal-extraction approach as an effective and rigorous tool for the analysis of discontinuities in the rectangular waveguide and in the NRD has been demonstrated.

REFERENCES

[1] J. A. G. Malherbe, "The design of a slot array in nonradiating dielectric waveguide: Part I—Theory," *IEEE Trans. Antennas Propagat.*, vol. AP-32, pp. 1335–1340, Dec. 1984.

[2] J. A. G. Malherbe, J. H. Cloete, I. E. Losch, M. W. Robson, and D. B. Davidson, "The design of a slot array in nonradiating dielectric waveguide: Part II—Experiment," *IEEE Trans. Antennas Propagat.*, vol. AP-32, pp. 1341–1344, Dec. 1984.

[3] B. Ghosh, L. Shafai, A. Ittipiboon, and D. J. Roscoe, "Slot array in nonradiating dielectric waveguide," in *IEEE AP-S Int. Symp. Dig.*, Montreal, QC, Canada, July 13–18, 1997, pp. 2508–2511.

[4] S. Haffa, D. Hollmann, and W. Wiesbeck, "The finite difference method for s-parameter calculation of arbitrary three-dimensional structures," *IEEE Trans. Microwave Theory Tech.*, vol. 40, pp. 1602–1610, Aug. 1992.

[5] N. Pena and M. M. Ney, "Absorbing-boundary conditions using perfectly matched-layer (PML) technique for three-dimensional TLM simulations," *IEEE Trans. Microwave Theory Tech.*, vol. 45, pp. 1749–1755, Oct. 1997.

[6] M. Righi and W. J. R. Hoefer, "Efficient 3D-SCN-TLM diakoptics for waveguide components," *IEEE Trans. Microwave Theory Tech.*, vol. 42, pp. 2381–2385, Dec. 1994.

[7] M. Righi, W. J. R. Hoefer, M. Mongiardo, and R. Sorrentino, "Efficient TLM diakoptics for separable structures," *IEEE Trans. Microwave Theory Tech.*, vol. 43, pp. 854–859, Apr. 1995.

[8] J. L. Dubard and D. Pompei, "A modified 3-D TLM variable node for the Berenger's perfectly matched layer implementation," in *13th Annu. Rev. Progress Appl. Computational Electromagnetics*, Monterey, CA, Mar. 17–21, 1997, pp. 661–665.

[9] ——, "Simulation of Berenger's perfectly matched layer with a modified TLM node," *Proc. Inst. Elect. Eng.*, pt. H, vol. 144, no. 3, pp. 205–207, June 1997.

[10] B. Ghosh, N. Simons, L. Shafai, A. Ittipiboon, A. Petosa, and M. Cuhaci, "Extraction of scattering matrix coefficients of NRD and waveguide discontinuities by the TLM method," in *Antenna Technol. and Appl. Electromagnetics Symp.*, Ottawa, ON, Canada, Aug. 9–12, 1998, pp. 535–538.

[11] N. Marcuvitz, *Waveguide Handbook*. Boston, MA: Boston Technical Publishers, 1964.

[12] N. R. S. Simons, R. Siushansian, J. LoVetri, and M. Cuhaci, "Comparison of the TLM and FDTD methods for a problem containing a sharp metallic edge," *IEEE Trans. Microwave Theory Tech.*, vol. 47, pp. 2042–2045, Oct. 1999.

[13] R. F. Harrington, *Time–Harmonic Electromagnetic Fields*. New York: McGraw-Hill, 1961.

[14] B. Ghosh, N. Simons, L. Shafai, A. Ittipiboon, A. Petosa, and M. Cuhaci, "Modal extraction for a slot in an NRD ground plane using the transmission line matrix method," in *URSI Nat. Radiation Sci. Meeting*, Orlando, FL, July 11–16, 1999, p. 99.

[15] C. Di Nallo, F. Frezza, A. Galli, P. Lampariello, and A. A. Oliner, "Properties of NRD-guide and H-guide higher-order modes: Physical and nonphysical ranges," *IEEE Trans. Microwave Theory Tech.*, vol. 42, pp. 2429–2434, Dec. 1994.

[16] C. Di Nallo, F. Frezza, A. Galli, G. Gerosa, and P. Lampariello, "Radiation modes, leaky waves, and Dyadic Green's functions in nonradiative-dielectric waveguide," in *Proc. Asia–Pacific Microwave Conf.*, vol. 1, 1993, pp. 5/23–5/26.

[17] F. Boone and K. Wu, "Mode conversion and design consideration of integrated nonradiative dielectric (NRD) components and discontinuities," *IEEE Trans. Microwave Theory Tech.*, vol. 48, pp. 482–492, Apr. 2000.

Bratin Ghosh was born in Calcutta, India, on July 1, 1968. He received the B.E. degree in electronics and telecommunication engineering from Jadavpur University, Calcutta, India, in 1990, the M.Tech. degree in microwave engineering from the Indian Institute of Technology, Kharagpur, India, in 1994, and is currently working toward the Ph.D. program in applied electromagnetics at the University of Manitoba, Winnipeg, MB, Canada.

His current research interests are numerical techniques in electromagnetics and low-loss millimeter-wave components and systems.

Mr. Ghosh was a recipient of a 1997 University of Manitoba Graduate Fellowship.

Neil R. S. Simons received the B.Sc. (with distinction), M.Sc., and Ph.D. degrees in electrical engineering from the University of Manitoba, Winnipeg, MB, Canada, in 1987, 1990, and 1994, respectively, and the Masters degree in mathematical finance from the University of Toronto, Toronto, ON, Canada, in 2000.

From 1987 to 1989, he was with Quantic Laboratories, Winnipeg, MB, Canada, where he was involved with problems related to transmission-line effects on printed circuit boards. From 1994 to 1999, he was a Research Scientist in the Antennas and Component Integration Group, Communications Research Centre, Ottawa, ON, Canada. He is currently Manager, Market Risk Trading and Insurance with the Royal Bank of Canada, Toronto, ON, Canada. His research has included the application of the TLM method to antennas and microwave circuits, and the application of lattice gas automata and special-purpose computers to solving electromagnetic-field problems.

Lotfollah Shafai (S'67–M'69–SM'75–F'88) received the B.Sc. degree from the University of Tehran, Tehran, Iran, in 1963, and the M.Sc. and Ph.D. degrees in applied sciences and engineering from the University of Toronto, Toronto, ON, Canada, in 1966 and 1969, all in electrical engineering.

In November 1969, he joined the Department of Electrical and Computer Engineering, University of Manitoba, Winnipeg, MB, Canada, as a Sessional Lecturer, Assistant Professor (1970), Associate Professor (1973), and Professor (1979). Since 1975, he has made special effort to link the University of Manitoba research to industrial development by assisting industries in the development of new products or establishing new technologies. In 1985, in an effort to enhance the University of Manitoba contact with industry, he assisted in establishing "The Institute for Technology Development," and was its Director until 1987, when he became the Head of the Electrical Engineering Department. His assistance to industry was instrumental in establishing an Industrial Research Chair in Applied Electromagnetics at the University of Manitoba in 1989, which he held until July 1994.

Dr. Shafai is a Fellow of The Royal Society of Canada since 1998. He has been a participant in nearly all IEEE Antennas and Propagation Society (IEEE AP-S) symposia and participates on the review committees. He is a member of URSI Commission B and was its chairman from 1985 to 1988. In 1986, he established the Symposium on Antenna Technology and Applied Electromagnetics (ANTEM) at the University of Manitoba, which is currently held every two years. He has been the recipient of numerous awards. In 1978, his contribution to the design of a small ground station for the Hermus satellite was selected as the Third Meritorious Industrial Design. He was the recipient of the 1984 Professional Engineers Merit Award. In 1985, he was the recipient of The Thinker Award presented by the Canadian Patents and Development Corporation. He was the recipient of 1983, 1987, and 1989 Research Awards presented by the University of Manitoba, the 1987 Outreach Award, and the 1989 Sigma Xi Senior Scientist Award. He was the recipient of the 1990 Maxwell Premium Award presented by the Institution of Electrical Engineers (IEE), U.K., and the 1993 and 1994 Distinguished Achievement Awards presented by the Corporate Higher Education Forum. He was the recipient of the 1998 Winnipeg RH Institute Foundation Medal for Excellence in Research. He was also the recipient of the 1999 University of Manitoba, Faculty Association Research Award.

Apisak Ittipiboon (M'80) received the B.E. degree (with honors) from Khonkaen University, Khonkaen, Thailand, in 1971, and the M.Sc. and the Ph.D. degrees in electrical engineering from the University of Manitoba, Winnipeg, MB, Canada, in 1971 and 1980, respectively.

Since 1985, he has been with the Communications Research Centre, Ottawa, ON, Canada, where he is currently a Senior Antenna Research Scientist and a Project Leader. He is also an Adjunct Professor with Electrical and Computer Engineering Department, University of Manitoba, Winnipeg, MB, Canada. His current research includes low-profile high-gain leaky-wave and holographic antennas. He has been involved in research and development on dielectric-resonator antennas, active phased arrays, and planar lenses. His interests include applied electromagnetics, waves on periodic structures, millimeter-wave technology and devices, and wireless communications.

Aldo Petosa (S'88–M'95) received the B.Eng, M.Eng., and Ph.D. degrees in electrical engineering from Carleton University, Ottawa, ON, Canada, in 1989, 1991, and 1995, respectively.

From 1990 to 1994, he was with the CAL Corporation, Ottawa, ON, Canada, where he was involved with research on novel microstrip antennas for cellular and mobile satellite communication applications. In 1994, he began his own company, Far Field, to market antenna-engineering software for computer-aided design of antennas and arrays. In 1995, he was involved with the development of planar base-station antennas for personal communication systems at GANDEC Systems Inc., Ottawa, ON, Canada. He is currently the Project Leader in Antenna Design and Development with the Advanced Antenna Technology Laboratory, Communications Research Centre, Ottawa, ON, Canada, where he is involved with various projects involving a wide range of antennas and arrays, including multilayer microstrip antennas, dielectric lenses, holographic antennas, and dielectric resonator antennas. He is also an Adjunct Professor with the Department of Electronics, Carleton University.